Available online at www.sciencedirect.com
ScienceDirect
Trans. Nonferrous Met. Soc. China 34(2024) 1634−1654
Transactions of Nonferrous Metals Society of China
www.tnmsc.cn

A review of preparing high-purity metals by vacuum distillation

Zhi-peng XU, Li-li JIA, Zhi-qiang HE, Xue-yi GUO, Qing-hua TIAN

School of Metallurgy and Environment, Central South University, Changsha 410083, China

Received 24 October 2022; accepted 12 May 2023

Abstract: With the development of science and technology, the high-tech industry has increasingly higher requirements for the purity of metals. However, the presence of trace impurities can have a bad effect on the properties of metals. Vacuum distillation process is widely used to prepare high-purity metals because of its advantages of high metal recovery, good environmental protection and simple equipment. In this paper, the overall progress in the preparation of high-purity metals around the principle and process research of vacuum distillation is systematically summarized. Principles of vacuum distillation, variant design of vacuum distillation, parameter optimization and simulation are covered. Based on the current status of the preparation of high-purity metals by this technology, it is pointed out that mechanistic studies and simulations are indispensable in scientific research. This research has certain reference significance for improving production efficiency, saving production cost and improving metal purity.
Key words: vacuum distillation; high-purity metal; theoretical calculation; process study; simulation

1 Introduction

High-purity metal is generally not less than 5 N (99.999% purity). Due to its special metal properties, it is of great significance in scientific research and industrial applications. Common high-purity metals include high-purity aluminum, high-purity magnesium, high-purity gallium, high-purity indium, and high-purity tellurium. Table 1 [1−8] lists common high-purity metals and their application fields. In addition, high-purity metals can also be alloyed as additives to enhance their properties [9−11]. Therefore, the development of high technology has a great dependence on the availability of high-purity metals.

In recent years, the demand for high-purity metals in high-tech industries has increased dramatically. The output of many metals, such as primary aluminum, copper, lead, zinc, and nickel, has been lower than the demand. Taking 2021 as an example, the world's average annual production and demand for some metals published by the World Bureau of Metal Statistics is shown in Fig. 1 [12]. It can be seen from the figure that the demand for aluminum, copper, lead, nickel, and other metals in 2021 is more than the production for them.

As demand continues to increase, efficient production methods are required to support the development of new technologies [13]. The purification of high-purity metals mainly includes chemical refining methods [14,15] and physical refining methods [16,17]. The purity of the product is limited to chemical refining. Physical methods are the most commonly used in the preparation of high purity metals. Vacuum distillation, zone melting and Czochralski crystal growth are the main methods [18].

Although the zone smelting method has the advantages of wide adaptability, simple equipment operation and high product purity, this method is not suitable for impurities which have a distribution coefficient close to 1 [19]. Traditional zone smelting technology obviously limits its further

Corresponding author: Qing-hua TIAN, Tel: +86-18684718188, E-mail: qinghua@csu.edu.cn
DOI: 10.1016/S1003-6326(24)66496-4

Table 1 Application of different high-purity metallic elements

Metal	Application	Metal	Application
Al [1]	Manufacturing of electronic devices, integrated circuits, flexible packaging, and labeling for food containers	In [5]	Flat panel displays, fiber optics, and various electronics
Mg [2]	Magnesium-based medical implants, battery negative replacement	Cu [6]	Integrated circuits and transistors
Te [3]	Semiconductor compounds for electronic and optical devices	Sb [7]	Flame retardant, used as a dopant in III−V semiconductor materials for infrared detectors, diodes, and hall effect devices
Ga [4]	Starting materials for epitaxial semiconductor crystal growth	Cd [8]	Solders mainly used in semiconductor processing and compound semiconductors such as CdS

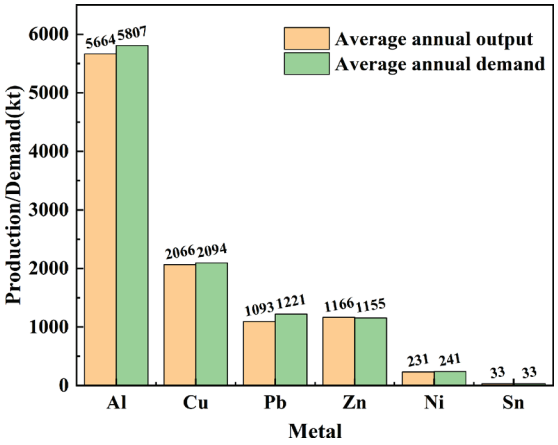

Fig. 1 Supply and demand for metals worldwide in 2021 [12]

development [20]. Czochralski crystal growth method, also known as the CZ method, is the most important method for making large semiconductor wafers for electronic applications [21,22]. But the raw material crystals are complicated, and it is difficult to pull out single crystals. On the other hand, to suppress the volatilization of the matrix metal, the performance of the device required for purification is high. The principles of zone melting and Czochralski crystal growth method are shown in Fig. 2 [23,24].

Vacuum distillation is considered to be the most effective method for metal purification due to reducing reaction temperature and effectively reducing the adverse effects of the gas [25]. It has been widely used in the field of metallurgical purification. In this paper the overall progress of research related to the preparation of high-purity metals by vacuum distillation is mainly summarized. The principle, variant design of vacuum distillation, parameter optimization, and simulation of vacuum distillation are introduced. This research can provide

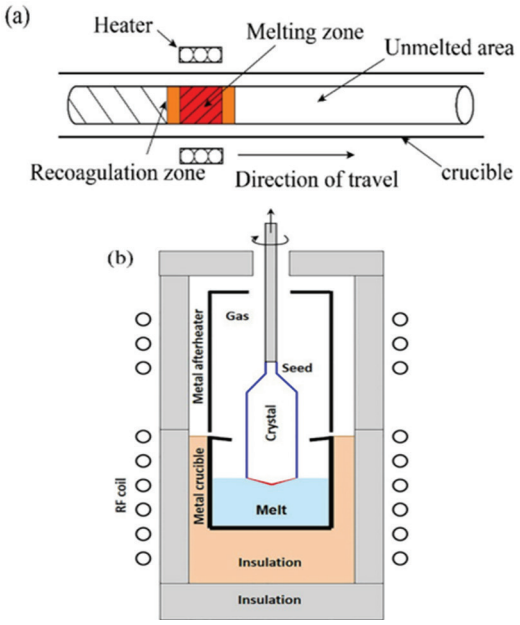

Fig. 2 Principles of purification technology: (a) Zone melting; (b) Czochralski crystal growth method (Reprinted with permission from [23,24])

a reference for future experiments on purifying metals by vacuum distillation.

2 Mechanism of vacuum distillation

Different metals have different saturated vapor pressures when the same temperature is set under airtight conditions. Vacuum distillation uses this principle to separate the matrix metal and impurities. The principle of vacuum distillation is shown in Fig. 3. In the vacuum heating environment, the impurities with high saturated vapor pressure first volatilize into the gas phase, and then the vapor becomes solid crystals under the condensation and adheres to the tube wall of the condenser tube. Impurities with relatively low vapor pressure will remain in the crucible at the bottom of the vacuum

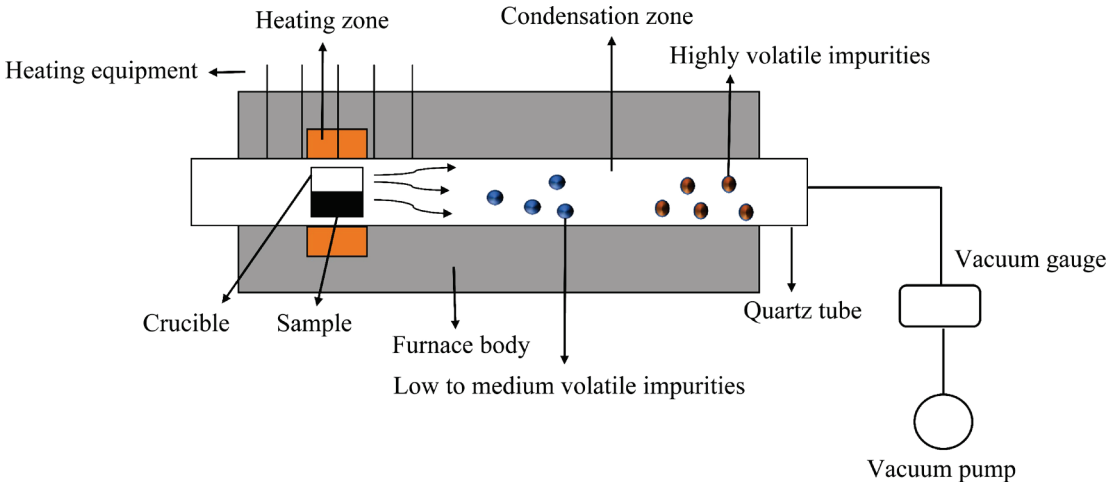

Fig. 3 Principle of vacuum distillation

distillation equipment. Matrix metal achieves purification in this way. Vacuum distillation has the advantages of a short process, high efficiency, and environmental protection. In addition, it can keep up with the demand for energy-saving and clean production. It has been widely used in alloy separation and secondary resource recovery [26].

2.1 Basic equations

2.1.1 Saturated vapor pressure

Different metals have different saturated vapor pressures when the same temperature is set under airtight conditions. According to this principle, it is possible to preliminarily judge whether impurities can be separated from the matrix metal in the vacuum purification experiments of metals. The impurities with saturated vapor pressures higher than the matrix metal enter the gas phase earlier. In contrast, impurities with low saturated vapor pressure remain in the melt and finally remain in the crucible residue to achieve separation.

ALCOCK et al [27] studied the metal vapor pressure equation and finally obtained the Antoine equation to calculate the saturated vapor pressure:

$$\lg p=A+BT^{-1}+C\lg T+10^{-3}DT \quad (1)$$

where p is the saturated vapor pressure of pure metal, T is the temperature, and A, B, C, and D are constants determined for each impurity. For each element, the constant value corresponding to the equation is based on a new evaluation of thermochemical data for the condensed and gaseous elements. However, this equation only works for $(1.013\times10^{-10}–1.013\times10^{2})$ Pa, and the precision of the equation is lower.

It is assumed that the impurities in high-purity metals are mainly in the form of simple substances. The effect of the simple substance form of impurities on the experimental results can be calculated from thermodynamic data. The relevant thermodynamic data are simple and easy to obtain, and the prediction effect is accurate in a large number of experiments. Most researchers use the thermodynamic Clausius Clapeyron equation to calculate the saturated vapor pressure of pure metals in the experiment [28]:

$$\lg p=A_1T^{-1}+B_1\lg T+C_1T+D_1 \quad (2)$$

where A_1, B_1, C_1, and D_1 are constants, which can be obtained by looking up the relevant thermodynamics manual. The equation takes into account the more practical situation: the latent heat of evaporation varies with temperature. Therefore, it is widely used to predict whether the impurities can be effectively separated in vacuum distillation. Taking crude selenium purification as an example, Fig. 4 [29] shows the saturated vapor pressures of selenium and impurities (Pb, PbSe, and PbTe) at different temperatures. The saturated vapor pressures of Se, Pb, PbSe, and PbTe increase gradually with increasing temperature. It is generally believed that materials with higher vapor pressures are more volatile [29]. Within the experimental temperature range, impurities with a lower saturated vapor pressure than selenium are likely to remain in the residue. Compared with other impurities, the saturated steam pressure of Pb

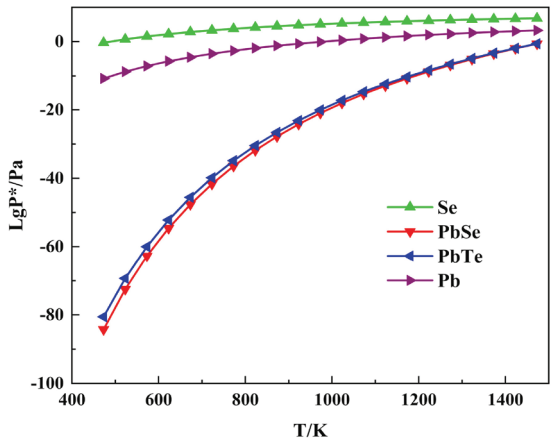

Fig. 4 Calculated saturated vapor pressure of Se and impurities Pb, PbSe and PbTe at different temperatures (Reprinted with permission from [29])

is the most similar to that of Se, which is not easy to remove.

2.1.2 Separation coefficient

The saturated vapor pressure is only used to preliminarily judge whether separation between impurities and the matrix metal. The separation coefficient (β_i) is often used to express the degree of separation of impurities in the vacuum distillation process. When $\beta_i>1$, the composition of the element in the gas phase is greater than that in the liquid phase, and when $\beta_i<1$, the composition of the element in the liquid phase is greater than that in the gas phase. The above two types of impurity elements can be separated from the matrix metal. When β_i is close to 1, the distribution of impurities in the gas and liquid phase is equivalent, so it is difficult to separate the impurities by vacuum distillation. Based on the separation coefficient of the impurities, the farther the separation coefficient is from 1, the easier it is to separate the impurities from the matrix metal. The separation coefficient of impurity element i can be calculated by Eq. (3) [30]:

$$\beta_i=\frac{\gamma_i}{\gamma_A}\times\frac{p_i}{p_A} \tag{3}$$

where γ_i and γ_A represent the activity coefficients of impurity i and matrix metal A, respectively. p_i and p_A represent the saturated vapor pressures of impurity i and matrix metal A, respectively. This equation is currently considered to be the most reliable method for calculating the separation coefficient. What is more difficult is that a large number of models are required to calculate the activity coefficients of matrix metals and impurities in this method. Many related parameters which are not easy to obtain are needed to calculate the activity coefficient of a binary system. This method of calculating the separation coefficient has only been applied to a few metal systems such as tin, iron and copper because of the difficulty of calculation.

With the development of vacuum distillation technology to prepare high-purity metals, simpler formulas were derived during a large number of experiments. ZHANG et al [31] proposed a revised separation coefficient equation through vacuum distillation purification experiments and theoretical analysis. The modified separation coefficient (β') equation is as follows:

$$\beta'=\frac{E_i}{E_A}=\frac{p_i^{\Theta}}{p_A^{\Theta}}\sqrt{\frac{M_i}{M_A}} \tag{4}$$

where E_A and E_i represent the distillation rates of the matrix metal and the impurities, respectively. p_A^{Θ} and p_i^{Θ} represent the vapor pressures of the matrix metal and impurities in standard conditions, respectively. M_A and M_i represent the atomic masses of the matrix metal and impurities, respectively. The equation for distillation rate (E) is as follows:

$$E=4.37\times10^{-4}\,p\sqrt{M/T} \tag{5}$$

where M is the relative atomic mass. This method is only applicable to impurities with separation coefficient less than 1, and there is a large deviation in the calculation of other impurities.

Another calculation method of the separation coefficient when studying the volatilization of a small amount of impurities in steel is obtained, which is based on the empirical Eq. (6) [32]:

$$y_i=100-100\left(1-\frac{x_A}{100}\right)^{\alpha_i} \tag{6}$$

where x_A and y_i represent the evaporation mass percentage of the matrix metal and impurities, respectively. α_i is the evaporation coefficient of impurities. Substitute the obtained evaporation coefficient into Eq. (7) to calculate the separation coefficient [32]:

$$\beta_i=\alpha_i\sqrt{\frac{M_i}{M_A}} \tag{7}$$

If the evaporation rates of the matrix metal and impurities are known, the evaporation coefficients of impurities can be obtained, and then the separation coefficients and activity coefficients of impurities can be obtained. Compared with the previous two methods of calculation, this method requires less related parameters and the calculation is simpler. In addition, the calculation of this equation is more accurate for the prediction of the separation effect of most of the impurities.

CHURBANOV et al [33] pointed out that the study of the effective separation coefficient (α) can describe the behavior of impurities in the vacuum distillation process. The removal rates of impurities can be characterized by calculation. The equation for the effective separation coefficient α is as follows:

$$\ln\left(\frac{n_0 m_i}{n_0 m_0 + n_d m_d}\right)=\frac{\alpha-1}{\alpha}\ln\frac{m_i}{m_0} \tag{8}$$

where n_0 and n_d represent the densities of particles in the residue and fraction, respectively; m_i represents the initial mass of the sample; m_0 and m_d represent the masses of the residue and fraction, respectively. α is given by the Rayleigh equation for high boiling impurities. Through the comparison between the experimental results and the theoretical calculation results, it is found that the relative uncertainty of the effective separation coefficient α obtained from the above equation is not satisfactory. Among the existing separation coefficient calculation methods, the calculation results of the two methods represented by Eq. (3), and Eqs. (6) and (7) are the most accurate in the theoretical calculation of high-purity metal preparation. It is still hard for researchers to get the relevant parameters required for calculation.

2.1.3 Evaporation rate

In addition to the above process parameters used to predict the experimental effect of vacuum distillation to prepare high-purity metals, the evaporation rate can reflect the experimental effect. The evaporation rate indicates the degree of evaporation of metal to be purified. By understanding the evaporation rate of metal elements, the time required for distillation can be calculated to reduce unnecessary energy consumption and improve production efficiency. Evaporation rate is usually calculated by dividing the mass of the distillate by the mass of the raw material. PRASAD et al [34] calculated the evaporation rate using the following equation:

$$\alpha_A=5.83\times10^{-2}P_A(M_A/T)^{1/2}f \tag{9}$$

where f is the probability that the metal molecule of the substrate is on the melting surface and is approximately 1. The experimentally obtained evaporation rate is approximately three orders of magnitude lower than the theoretically calculated evaporation rate using the above equation. Different from the previous equation, ZAIOUR et al [3] used a new equation to calculate the evaporation rate of impurities in the preparation of 7N tellurium by vacuum distillation:

$$\alpha_i=\frac{1}{S}\frac{\mathrm{d}m_i}{\mathrm{d}t}=-0.0583\beta P_A\left(\frac{vM_i}{l}\right)^{1/2}f \tag{10}$$

where S is the evaporation area, t is the distillation time, β is the Langmuir coefficient, v represents the atomic number of evaporated impurities, and l represents the length of the melting zone. The impurity evaporation rate calculated by this equation is 3.35×10^{-2} kg/(m^2·s), while the experimentally determined average evaporation rate is 1×10^{-3} kg/(m^2·s). The actual evaporation rate is reduced, due to the presence of non-volatile impurities in the molten fraction which interfere with the evaporation of volatile impurities. Therefore, it is also the academic pursuit of researchers to establish an impurity evaporation rate equation that conforms to the experimental effect.

2.1.4 Molecular mean free path

In the process of vacuum distillation, the impurities that reach the saturated vapor pressure will be the first to evaporate. By comparing the molecular average free path of the vapor with the effective size of the system, it is possible to judge how the impurities evaporate during the distillation process. Calculating the mean free path of molecules can help us better analyze the experimental results. The mean free path (λ) can be calculated as [34]

$$\lambda=2.33\times10^{-20}T/(\xi^2P) \tag{11}$$

where ξ is the diameter of the vapor molecule (cm); P is the chamber pressure. The mean free path λ is usually compared with the effective size (D) of the vessel to determine the thermal path of gas

molecules during vacuum distillation. The effective size of vessel D is generally considered to be the distance between the surfaces of the melt and the condenser. When $\lambda \ll D$ the distillation process is the "viscous" type, and when $\lambda \gg D$, the distillation process is a type of molecular distillation; anything in-between belongs to viscous−molecular flow. The molecular path can be obtained by calculating the molecular free path of each component in the vacuum distillation system at a specific temperature and different pressures [35]. Figure 5 [35] shows the molecular free path of each vapor molecule in copper anode slime at 1273 K under different pressures. It can be seen from the figure that the molecular free path of vapor molecules decreases with increasing system pressure. The smaller the system pressure is, the more obvious the difference in the free path is. Metals volatilize from the material, resulting in differences in element distribution during vapor condensation due to differences in the free path of each molecule. Under the same pressure, S, Se and Te have more degrees of freedom than Pb, Sb and Bi, so they will move farther. By comparing the free path of different elements under the same experimental conditions, the type of molecular distillation can be roughly judged, and a better explanation for the distillation process can be made.

2.1.5 Calculation of Gibbs free energy change

In most cases, the impurities in the raw materials used in distillation will not exist in the form of elemental substances. Different elements combine with each other to form various compounds. To judge whether there is a reaction between different compounds, it is necessary to introduce Gibbs free energy [36]. The change in Gibbs free energy (ΔG) is used to determine whether a reaction will occur. When ΔG is a negative value, the reaction is spontaneous at a constant temperature and pressure. Conversely, when ΔG is greater than 0, the reaction is nonspontaneous [37,38]. ΔG can be expressed by Eq. (12):

$$\Delta G=\Delta G^{\Theta}+RT\ln Q \quad (12)$$

where ΔG^{Θ} is the standard Gibbs free energy change at atmospheric pressure, R is the general gas constant, and Q is the reaction entropy. Taking vacuum distillation to extract metallic silver and copper from secondary resources as an example, in Fig. 6 [39], the Gibbs free energy change of Cu_2Sb is less than 0 when the temperature is greater than 1504.79 K under a system pressure of 10 Pa. When the temperature is greater than 1391.61 K, the Gibbs free energy of Ag_3Sb is less than 0. The Gibbs free energy change of the two reactions decreases with increasing temperature. It can be seen that within the experimental temperature range, Ag_3Sb is easier to decompose than Cu_2Sb [39].

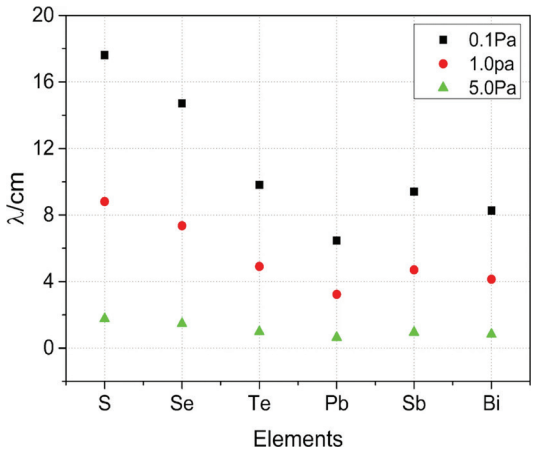

Fig. 5 Free paths of elements at different pressures at 1273 K (Reprinted with permission from [35])

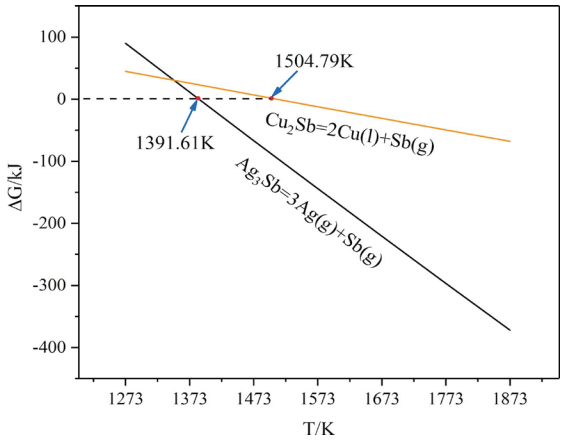

Fig. 6 Relationship between ΔG and temperature (10 Pa) (Reprinted with permission from [39])

2.1.6 Vapor−liquid equilibrium diagram

Reliable vapor−liquid equilibrium (VLE) is a necessary condition to determine the temperature requirements and separation efficiency [40]. To quantitatively analyze the distribution of various elements in the two phases of vapor and liquid in the vacuum distillation process, the VLE diagram is introduced to predict the separation effect. This diagram can be utilized to analyze the change in the vapor−liquid phase distribution in the vacuum

distillation process with temperature and pressure. It is necessary to introduce a model to estimate the activity of binary or ternary systems composed of each impurity and main metals [41−45]. At present, the thermodynamic models applied to the activity prediction of components mainly include the regular solution model, Miedema model, molecular interaction volume model (MIVM), nonrandom two-liquid (NRTL) equation and Wilson equation.

YANG et al [46] proposed a method to calculate the vapor−liquid equilibrium phase diagram based on VLE calculations and the MIVM model. The results show that the calculated value of the lead content in the gas phase is inconsistent with the experimental value at higher temperatures. Based on the VLE theory, XU et al [47] calculated the VLE data of the Zn−Ni alloy using the Wilson equation, plotted the VLE phase diagram, and compared the results with the experimental values. The results show that the variation trend of the experimental values with temperature is consistent with that of the T−x−y phase diagram, but there is a deviation. For the case of low experimental temperature, the Wilson equation predicts poor results. By comparing the above thermodynamic models, in terms of model parameters, the NRTL equation and the normal solution model require the fewest parameters, the Miedema model and MIVM equation require more parameters, and the Wilson equation requires parameters between the above models. By calculating the activities of the four binary systems Bi−Pb, Bi−Sn, Cd−Pb and Pb−Sn under the full composition and the average deviation of the corresponding activities and comparing the activity predicted by the experiment and the model, the best prediction is the NRTL equation; the Miedema model is the worst, and the other models are between the NRTL equation and the Miedema model [48]. Based on the advantages and disadvantages of the above prediction models, researchers generally tend to explore the MIVM model and the Wilson model, which have been deeply developed in the field of related binary and ternary alloys such as tin, titanium, and lead [49,50].

The method of drawing the vapor−liquid equilibrium diagram by using the activity prediction model is that in an ideal state, the interaction between impurities, the loss in the vacuum distillation process and whether the vacuum distillation process has reached thermodynamic equilibrium should be considered in the actual analysis [51]. The specific model needs to be modified according to the specific conditions of the experiment.

2.2 Influencing factors

In the vacuum distillation experiment, within a certain vacuum degree range, the most obvious influencing factors are the distillation temperature and distillation time. GAO et al [52] used vacuum gasification directional condensation technology to extract tellurium from lead anode slime. The effects of distillation temperature and distillation time on the experimental separation are discussed. The experimental results show that the volatilization rate of the matrix metal increases gradually with increasing temperature. When the temperature reaches 1173 K, the volatilization rate is close to 100%. With the extension of the distillation time, the volatilization rate will gradually increase. The volatilization rate is as high as 92% when the distillation holding time is more than 50 min. Within 100−125 min, the substrate metal is completely volatilized. This shows that within a range of conditions, the volatilization rate of metals is proportional to the distillation temperature and holding time. In the process of vacuum distillation, the degree of vacuum can affect the purification effect, so we also need to choose the appropriate degree of vacuum. By increasing the degree of vacuum to a suitable range, the volatilization rate of some impurities can be reduced [53]. Exploring a suitable set of process parameters can maximize the efficiency of the process, while also maximizing the use of energy. The condensation temperature also affects the final form of purifying products [54]. When the condensation temperature is low, the metal near the condenser wall has poor gloss. The crystal grains on the other side are coarse, and the hardness does not meet the requirements. When the condensation temperature is high, the metal attached to the side near the condensation wall is prone to sintering, which affects the recovery rate and makes it difficult to clean the equipment later. Therefore, it is important to choose a suitable condensation temperature in the experiment.

In practical experiments, there is always a

gap between the experimental and theoretical calculation results. PRASAD et al [55] pointed out that the structure and material of cold fingers are key factors affecting the purification of metals by vacuum distillation. The cold finger materials commonly used to deposit gas phase impurities are mainly stainless steel, quartz alumina and copper. In the selection of cold finger materials, the properties of the main metals and impurities in the distillate should be considered to avoid the secondary pollution during the distillation process. Other parameters of the condensation finger, such as rotational speed, must be considered in the experiment [56].

In addition to the above factors, the types and contents of impurities in raw materials, the interaction between impurities in the distillation process, and the structure, materials and inevitable subjective factors of distillation equipment can lead to errors in the experiment [57−59]. This should be taken into account when analyzing the experimental data.

3 Design of vacuum distillation furnace

3.1 Basic structure of furnace

Vacuum distillation furnaces are divided into vertical and horizontal vacuum furnaces. Their basic structures are similar, mainly composed of a heating system, vacuum system, condensation system and collection system, and are equipped with gas pipelines outside the equipment. The difference is that the horizontal vacuum furnace avoids the influence of gravity on the volatilization of impurities. But it occupies a relatively large area. Two types of distillation furnaces are shown in Figs. 7 [33] and 8 [60].

3.2 Improvement of furnace

Vacuum distillation is a method of separating and purifying metals. The principle is that under closed conditions, different metal elements have different pressures when the gas phase and liquid phase reach equilibrium at the same temperature. Therefore, some impurities with similar melting points, boiling points or saturated vapor pressures cannot be effectively removed. A high-precision temperature control system needs to be set up to control the heating and condensation for better separation of impurities.

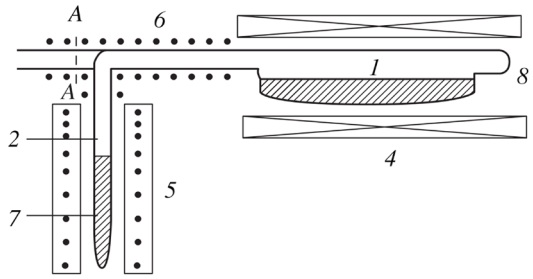

Fig. 7 Schematic diagram of vertical vacuum distillation furnace: 1−Distiller evaporator; 2−Receiver; 3−Two zone resistance furnace; 4−Evaporator resistance furnace; 5−Receiver gradient furnace; 6−Heater; 7−Distillate; 8−Carrying raw material pipe (Reprinted with permission from [33])

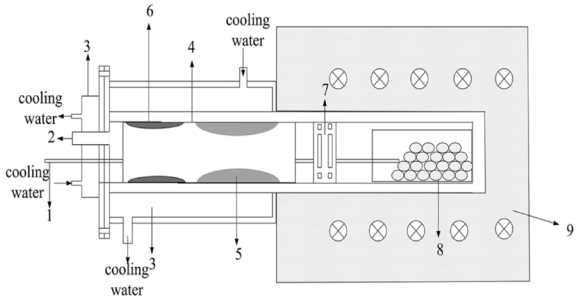

Fig. 8 Schematic diagram of vacuum thermal reduction kettle: 1−Thermocouple; 2−Vacuum tube; 3−Water cooling jacket; 4−Condenser; 5−Crystallized electrolyte; 6−Crystallized sodium; 7−Thermal fuse; 8−Raw material; 9−Furnace (Reprinted with permission from [60])

LIANG et al [61] designed a horizontal staged condensation vacuum furnace (see Fig. 9). The quartz tube, as the core of the horizontally staged condensation vacuum furnace, consists of two different parts: the volatilization zone on the left and the condensation zone on the right. When the volatilization zone is heated, a temperature field from high to low can be formed in the quartz tube. Elements such as K, Na, Zn and Mg can evaporate and undergo fractional condensation, and non-volatile impurities remain in the residue. Finally, the effective separation of different elements is realized. The device realizes the effective separation of magnesium and impurities by accurately controlling the evaporation and condensation process. The content of harmful impurity Fe is controlled at approximately 1×10^{-6} (mass fraction). The content of volatile impurity Zn, which is not easy to separate from magnesium, is also reduced to 1×10^{-6} (mass fraction).

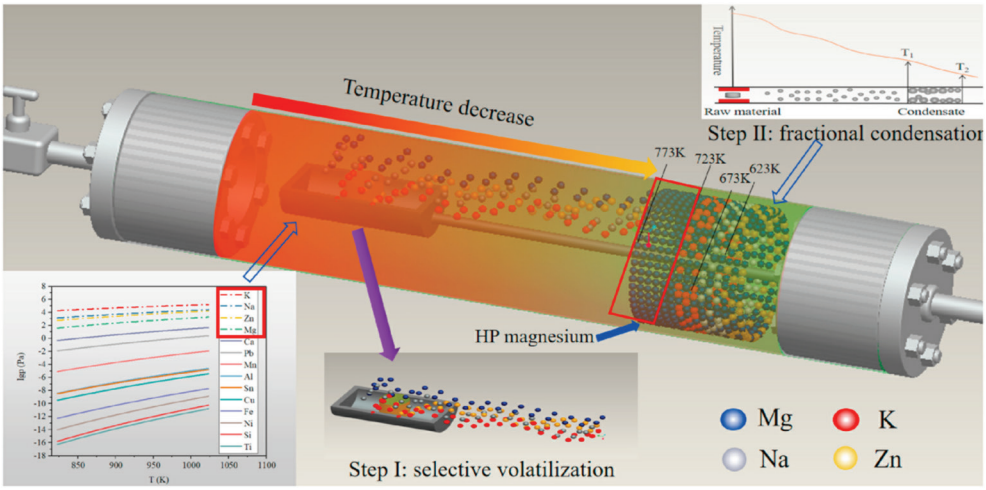

Fig. 9 Diagram of experimental setup (Reprinted with permission from [61])

During the distillation process, the migration of the metal layer at the vacuum interface is the key to affecting the evaporation rate of impurity elements. The diffusion rate has a more significant effect on the evaporation rate. In the absence of stirring, to make the metal melt have good mass transfer conditions, it is necessary to design an evaporator with a unique structure, and the concept of multistage evaporation comes into being. The multistage evaporator has good mass transfer and heat transfer conditions by changing the flow rate and the number of falls of the melt. After experimental verification, the Pb−Sn alloy with a Pb content of approximately 80 wt.% was distilled in a 5-level constant volume distillation furnace. Crude Sn with a Pb content of approximately 5 wt.% was obtained [62]. HAGEMAN et al [63] used specially designed quartz ampoules coupled to a permanent vacuum system. A final vacuum of approximately 1.33×10^{-5} Pa can be achieved on an empty ampoule using a turbo pump with a liquid nitrogen trap. During the experiment, a 1.33×10^{-4} Pa vacuum system was used for three-stage distillation. The average overall yield achieved for single-stage distillation was 84%, the average overall yield for two-stage distillation was 80%, and the average overall yield for three-stage distillation was 76%. After a three-level distillation process, 4N metal materials were purified to 6N. The unique quartz design allows residual material to be removed between distillation stages. The product purity was improved by avoiding product exposure to atmospheric conditions. The purification material does not need to be processed, making the operation more convenient. A schematic diagram of the three-stage distillation tube is shown in Fig. 10 [63].

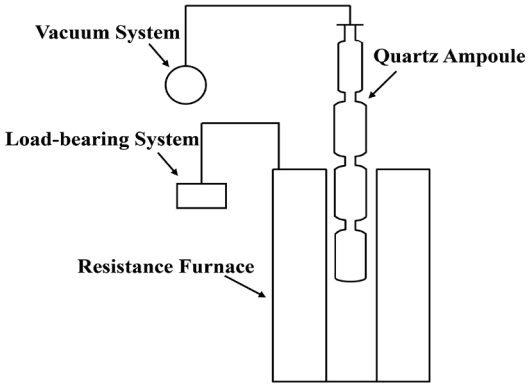

Fig. 10 Three-stage distillation device diagram (Adapted from [63])

Researchers have developed a new type of vacuum thermal reheating furnace (Fig. 11 [64]) because vacuum distillation equipment cannot monitor the changes in raw materials in real time during the experiment. When the material undergoes vacuum distillation, small changes in mass, pressure and temperature in the system can be recorded by the scale, vacuum gauge and thermocouple, respectively. Then, the signal is transmitted to the computer terminal. The actual experimental evaporation rate can be obtained by measuring the mass change of the material per unit time and area during the actual distillation process. In addition, DENG et al [65] have developed a continuous vacuum distillation furnace (Fig. 12). The material is first put into the material tank and then melted into the furnace through the top of

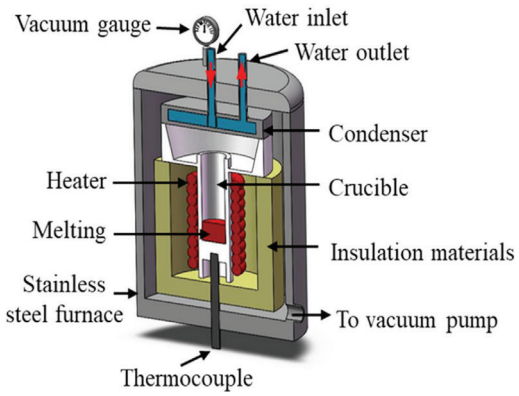

Fig. 11 Schematic diagram of vacuum thermogravimetric analysis furnace (Reprinted with permission from [64])

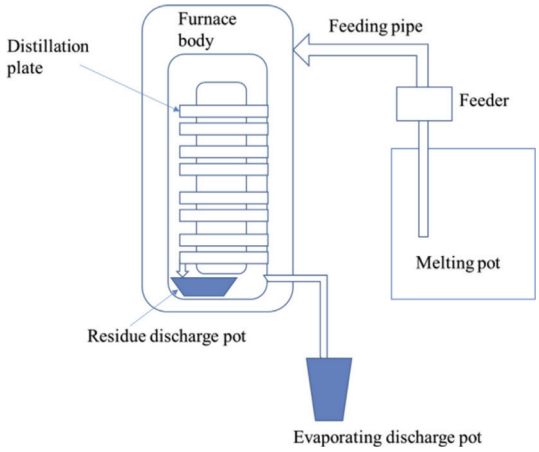

Fig. 12 Vertical continuous vacuum distillation furnace (Reprinted with permission from [65])

the equipment through the vacuum furnace feeder to realize the continuous feeding process. After entering the furnace through the multistage distillation tray, the residue falls to the bottom. Volatiles are released from the sides of the condensing unit. The device realizes the continuous inflow of materials and the continuous outflow of products, which improves the operation efficiency to a certain extent.

In order to achieve the effect of high efficiency and energy saving, researchers have been committed to the continuous improvement of equipment. In addition to the traditional vacuum distillation furnace, researchers are more inclined to combine vacuum distillation technology with other purification technologies. With the development of scientific research, various new vacuum distillation equipments have been developed. For example, combining vacuum distillation and vacuum electromagnetic refining technology, its principle is to use the electromagnetism of electromagnetic induction to suspend the metal materials in the quartz tube. The impurities will volatilize more fully under the heating and stirring of electromagnetic induction. It can also avoid the contamination of the material by the crucible [66].

4 Measures to improve efficiency of vacuum distillation

4.1 Multistage distillation

Based on the analysis of the mechanism and influencing factors of vacuum distillation, many researchers have devoted themselves to improving the efficiency of vacuum distillation and realizing green and efficient production. In addition to performing vacuum distillation experiments under optimal process conditions, multiple partial vaporizations and condensations of raw materials can also greatly improve the purity of the product. Distillation temperature and holding time can be set according to material composition and properties during each distillation process.

ZHANG et al [67] proposed the application of the multistage vacuum distillation in secondary resource recovery: a potential recovery method of cadmium telluride photovoltaic waste. Since the saturated vapor pressure of the matrix metal tellurium is much higher than that of the impurities at the same temperature, the matrix metal can evaporate at a relatively low temperature. Three-stage vacuum distillation is used in this process. The first-stage distillation temperature is 700 °C, the vacuum degree is 15 Pa, and the holding time is 40 min. The distillation temperature of the second stage is 450 °C, the holding time is 20 min, and the vacuum degree is 15 Pa. In the third stage, the temperature is kept at 400 °C, and the holding time is 20 min. The second (HTVD) and third-stage (LTVD) impurity separations are shown in Fig. 13 [69]. In the first-stage distillation stage, the matrix metal is evaporated to the maximum extent at high temperature. In order to remove impurities in the rear section, the impurity content in the rectification product of the first section should not be controlled too high. The purpose of the second stage of vacuum distillation is to remove cadmium at high temperature. The third stage of vacuum distillation is to remove sulfur at low temperature. At high vapor pressures, low-boiling metals can be

separated from other metals by distillation or sublimation. Metal evaporated into the gas phase is condensed to affect separation. The results show that the purity of the matrix metal can reach 99.97%, and the recovery rate can reach more than 99%. The contents of cadmium and sulfur in distillation products are 0.0061 wt.% and 0.0194 wt.%, respectively. At the same time, vacuum distillation can enrich the cadmium sulfide produced in the smelting process, and the purity can reach 99.6%.

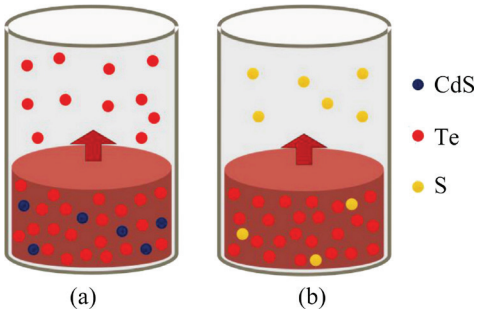

Fig. 13 Schematic diagram of the separation of impurity elements using (a) HTVD and (b) LTVD (Reprinted with permission from [67])

For the purification of metals by multistage distillation, in addition to the abovementioned method of first high-temperature distillation and then low-temperature distillation, a process of first low-temperature distillation and then high-temperature distillation can also be adopted. The first low-temperature distillation removes most of the highly volatile impurities, and the raw material for the second high-temperature distillation comes from the product of the low-temperature distillation. The second high-temperature distillation removes most of the low-volatility impurities, thereby maximizing the purity of the product. In the experiment of purifying indium, the content of impurities was greatly reduced by this method of first low-temperature distillation and then high-temperature distillation, and the 2N raw material was successfully purified into 5N product. The flow chart of the secondary distillation experiment is shown in Fig. 14 [68].

Multistage distillation can effectively improve the product purity. The specific distillation scheme also needs to be formulated according to the composition and properties of the experimental raw materials.

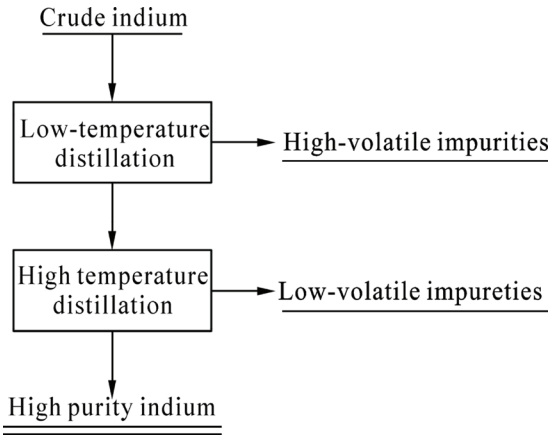

Fig. 14 Flow chart of the two-stage distillation experiment (Reprinted with permission from [68])

4.2 Removal of specific impurities

The type and content of impurities in the raw material can be analyzed from the raw material itself. Differences between the behavior of impurities were identified and impurities were separated through a series of calculations [69−71]. It is also helpful to analyze whether there are physical interactions and chemical reactions between different elements under experimental conditions [72−77]. HAGEMAN et al [63] improved the purity of tellurium from 5N to 6N. The most difficult impurity to remove is selenium. Its saturated vapor pressure at the same temperature is slightly higher than that of the matrix metal, so it will evaporate first. Additionally, the condensation temperatures for these materials are similar, minimizing the ability to remove selenium from the system. Given this disadvantage, SUN and ZHENG [78] proposed that selenium can be removed by bubbling hydrogen in molten tellurium to form selenium hydride and remove selenium together with hydrogen. The sample of vacuum distillation raw material contains 8.656×10^{-6} (mass fraction) impurities. The total impurity content of the product measured after hydrogenation is 0.92×10^{-6} (mass fraction). The selenium content is greatly reduced in this way.

Another promising method is to add an appropriate amount of elements to form intermetallic compounds or have high affinity with the elements to be removed [79,80]. This method can also prevent impurities from evaporating with matrix metal [81]. Taking crude antimony purification as an example, antimony and arsenic have similar

saturated vapor pressures at the same experimental temperature. These two elements will co-evaporate during vacuum distillation. It is difficult to remove arsenic only by vacuum distillation. Adding a certain amount of metal aluminum to the raw material can make aluminum and arsenic generate nonvolatile intermetallic compounds, thereby inhibiting the volatilization of arsenic. Experiments have shown that the content of arsenic in antimony products with additives is much lower than that in products without additives [82].

4.3 Establishment of impurity distribution model

There are a series of studies on high-purity metals prepared by vacuum distillation method. Nevertheless, only a few works have studied the impurity distribution in distillates. Because of the experimental principle of vacuum distillation, we cannot analyze the volatiles and distillate at any time during the experiment. The distilled products are evenly sampled according to the direction of crystal growth, and the distance from the sampling point to the condenser is approximately the distillation progress. The impurity distribution curve is obtained by analyzing the samples. The theoretical distribution models of impurities fill the research blank of impurity motion behavior and distribution in vacuum distillation process of high-purity metals [83−86].

An equation is derived for the impurity distribution in solidified distillates at a low impurity content and ideal stirring of the source material [87]. The impurity distribution is calculated by using the formula:

$$C/C_0=\beta[1-(x/L)]^{\beta-1} \tag{13}$$

where C is the concentration of the impurity at a distance from the condensing substrate of x, C_0 is the initial impurity concentration in the raw material, β is the separation coefficient, and L is the total length of the distillate. This formula assumes that α is close to 1 and the source material is ideally stirred. In particular, the distillation process in the apparatus is accompanied by revaporization both in the vapor line and from the condensate surface. As a result, the theoretical analysis and the actual situation of distillation-related processes are slightly different. The impurity distribution in the sublimation is calculated by applying the formula to the vacuum distillation of magnesium [88]. The Mn and Ca distributions can be described by a distillation equation. However, for most of the impurities, the distributions have a complex shape so that they cannot fit the theoretical curve completely.

ZHANG et al [89] proposed an improved separation coefficient in order to describe the impurity distribution more accurately. The modified separation coefficient is shown in Eq. (4). The distribution model is established as $C/C_0=\beta'[1-(x/L)]^{\beta'-1}$ to describe the fraction of the impurity distribution in the liquid. The results show that the calculated method of the separation coefficient of impurities in crude metal by the impurity content in distilled metal was not suitable for high-purity metals. This is because the calculation method is derived from sublimation theory. In contrast to the object being distilled, the substance being refined during sublimation is not actively mixed.

ZHANG et al [90,91] proposed a volatile distribution model for impurities based on the mass transfer rate equation and the law of conservation of mass in the liquid boundary layer. They built the distribution model of $C/C_0=k_{\text{eff}}\cdot[1-(x/L)]^{k_{[i]d}/k_{[m]e}}$ for highly volatile impurities and $C/C_0=k_{\text{eff}}[1-(x/L)]^{k_{\text{eff}}-1}$ for lowly volatile impurities in distillate. In these models, k_{eff} is the effective separation coefficient, $k_{[i]d}$ is the impurity mass-transfer coefficient in the liquid boundary layer, and $k_{[m]e}$ is the evaporation mass-transfer coefficient of the matrix metal. The former model is reliable in the direction of high purity metal preparation by vacuum distillation. Although there is a deviation between the calculated results and the experimental results, it provides a reference for the future model distribution.

In addition, it is also a good idea to combine vacuum distillation technology with other purification techniques [92−94]. Last but not least, the combination of vacuum distillation experiments and simulations is a big hot trend. The optimal parameter range of the experiment can be determined through simulation, which avoids wasting a lot of time in the process exploration experiment. It can also understand the real-time changes of the experiment, such as the reaction process and the temperature distribution of the material. The simulation results are different from the actual experiments because the simulation is

carried out under ideal conditions. Supplementing and optimizing the simulation model based on the experiment is a direction of future development.

5 Vacuum distillation simulation

Some researchers have studied the thermodynamics and dynamics of vacuum distillation technology. Through various software and mathematical models to simulate the experimental process, the experimenter can better understand the whole process of the experiment. The experimental parameters can be adjusted at any time to achieve the best vacuum distillation effect. With the development of computer technology, simulation has become a powerful tool [95,96].

5.1 Thermodynamic simulation

It is difficult to accurately measure the temperature in a vacuum distillation furnace in running mode in actual production. The existing temperature control model has uncertainty and serious delay [97−101]. It is not easy for traditional control methods to achieve precise control. The temperature distribution during the distillation process cannot be obtained intuitively either. Therefore, the thermodynamic simulation of the vacuum distillation process is developed [102−104]. There are three main heat transfer modes in vacuum distillation, which are heat conduction, heat convection and heat radiation. Heat transfer mainly occurs between the vacuum distillation furnace and the environment, the distillation furnace shell and the crucible, the crucible and the material. It is necessary to consider the changes of material temperature caused by three heat transfer modes in the simulation process.

LI et al [105] used CFX software to simulate the purification process of tellurium. The effects of the temperature gradient, argon flow rate and vacuum degree on the impurity diffusion and condensation are investigated. The established mathematical model takes into account distillation and multiphase models, and optimizes the Hertz−Langmuir equation based on gas dynamics theory. During the simulation, it is assumed that there is no additional gas flow other than the evaporation of impurities flowing in the unit. The total evaporation rate of the distillate in the system is represented in the diffusion model as a volumetric source term. It is assumed that the interfacial momentum, interfacial heat, and mass transfer depend directly on the contact surface area between the two phases. Additionally, the authors consider the heat transfer process on both sides of the phase interface and apply the thermal phase transition model to the condensation process. The experimental geometry and simulation grid are shown in Fig. 15 [105]. Different distillation conditions set through the CFX simulation show that the purification effect is consistent with the overall trend of the process parameters. It can be seen that it is feasible to simulate the vacuum distillation process by CFX software.

ZHANG et al [106] used the vapor pressure of metal Tm to determine the thermophysical parameters and sublimation temperature range of the Tm steam. The temperature distribution of the

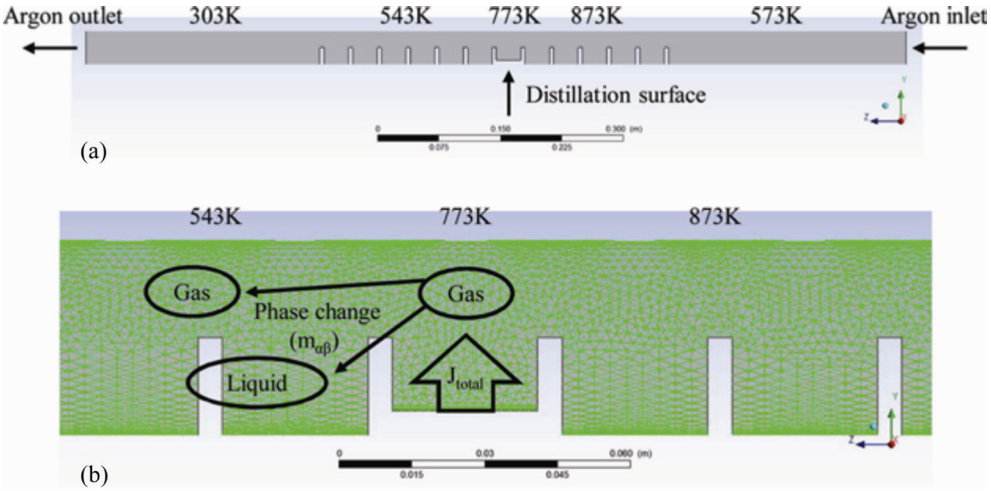

Fig. 15 Simplified geometry setup (a) and simulation mesh (b) for CFX simulation (Reprinted with permission from [105])

sublimation furnace at a heating body temperature of 1000 °C is studied by establishing a two-dimensional axisymmetric heat transfer model. The simulation results are shown in Fig. 16 [106]. Due to the heat loss at the bottom of the crucible, the temperature of the crucible, solid metal and Tm steam increase with increasing crucible height. The figure shows that the maximum value is reached at the middle of the crucible height direction and then drops rapidly. The surface temperature outside the condenser drops sharply, and the surface temperature and evaporation rate of the distillate can be obtained at the same time. The experimental process is clearer through this simulation. As early as 1996, a mathematical model of the pure metal vacuum distillation process was established, including the volatilization process, gas phase mass transfer process, condensation process and heat transfer process [107]. By solving the mathematical model with an iterative method, the evaporation rate of pure metal under different experimental temperatures and vacuum degrees can be obtained. This mathematical model is also widely used.

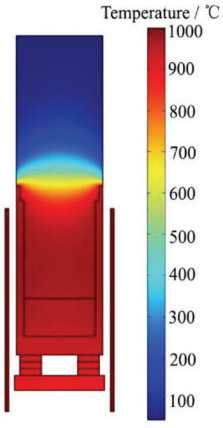

Fig. 16 Temperature in the sublimation furnace with a heating body temperature of 1000 °C (Reprinted with permission from [106])

XU et al [108] made a lot of efforts to solve the engineering problems such as long delay of the temperature control system and the difficulty of accurately measuring the real-time temperature. They found that PID genetic algorithm can effectively solve the delay problem of electric vacuum furnace. So the PID algorithm is widely used in industry. Unfortunately, the related algorithm easily falls into a local optimum, and there is no way to achieve the optimization goal in time. From this point, the PID model cannot be guaranteed to achieve the best performance [108]. WANG and LIU [109] proposed a modeling and calculation method for the temperature value of each node in the no-load furnace. The perturbation model for the temperature field of the system is established by the vacuum furnace itself. The distribution of the temperature field is simulated by controlling the temperature under the experimental conditions and ANSYS is used software to model and analyze the right half of the front view of the vacuum furnace. The thermal radiation simulation diagram of the vacuum furnace is shown in Fig. 17 [109]. By comparing the experimental results measured by the thermocouple sensor with the simulation results, the maximum relative error of the two is 3.696%, and the average relative error is 1.909%. The reason for this result is not only the error caused during the experiment but also the assumptions made in the early stage of the simulation. For example, the angle coefficient of radiation heat transfer is assumed to be equal. And only the heat radiation among the electric column, the heat conduction cover and the water-cooled furnace cover is considered. There is a deviation between the simulation results and the experimental results because the assumptions in the simulation cannot be realized in reality.

5.2 Dynamics simulation

The microstructure, thermodynamic properties, and internal transport properties of the melt not only affect the structures and properties of the synthetic materials, but also determine dynamics processes, such as separation and purification between metals [110]. The molecular dynamics method can not only be used to study the dislocations, defects and vacancies of pure metals but also calculate the thermodynamic properties of pure metals [111]. Molecular dynamics can be used to accurately simulate both macroscopic properties and microscopic information of the reaction system [112−114]. Therefore, dynamics and thermodynamic researches have become hotspots in the field of simulation. To study the dynamics of vacuum distillation to prepare high purity metals, the regularities of distribution of different impurities between evaporation and condensation are supplemented.

JIA et al [115] used the molecular dynamics

method to simulate the thermodynamic properties of Pb−Ag alloys in the temperature range of 298−1498 K. By calculating the excess free energy, condensation energy and formation energy of the system, the change in interatomic force with temperature during the experiment is reflected. This further reveals whether the heating operation is conducive to the evaporation and separation of metals. By comparing the simulation results with the experimental results, the relative errors of the excess free energy, condensation energy and formation energy are more than 1%. For the inevitable errors in the experimental process, the calculation model is not well avoided. The calculation of formation energy and cohesive energy is also applied to Si−Al alloy [116]. Deviation degree between the actual alloy and the ideal melt is quantitatively described by calculation. The interaction of atoms is strong in the process of vacuum distillation. As the temperature increases, the formation energy of the alloy continuously increases to about zero, which is close to the ideal melting state. This is consistent with the actual experimental phenomenon. Therefore, it is also a good method to calculate energy functions such as formation energy, cohesive energy and excess free energy.

The same CFD series software can also be used to study the kinetics of the vacuum distillation process. They can help us to understand the physical processes such as phase transition and metal solidification in the heating purification process [117]. Its modeling equations include the Navier–Stokes equation, energy equation and metal concentration equation. By modeling the vacuum distillation reactor, the temperature distributions under diffusion, natural convection and forced convection are simulated. The specific simulation distribution diagram is shown in Fig. 18 [117]. This figure explains the reasons for the product morphology and chemical composition. In addition, the distribution of impurity concentration with the distance of the reactor was also studied by simulation to compare whether there is forced convection on the surface of the molten metal at different distillation time. Through comparative

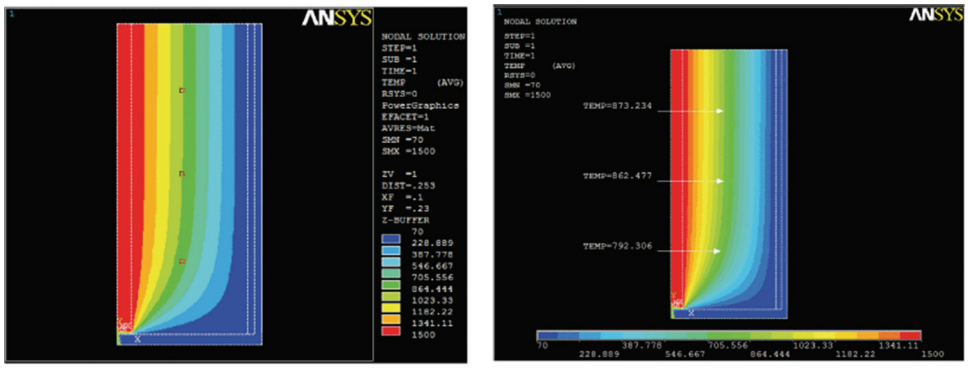

(a) Distribution of test nodes (b) Simulation results for node temperature

Fig. 17 Thermal radiation simulation of vacuum furnace model (right half front view, °C) (Reprinted with permission from [109])

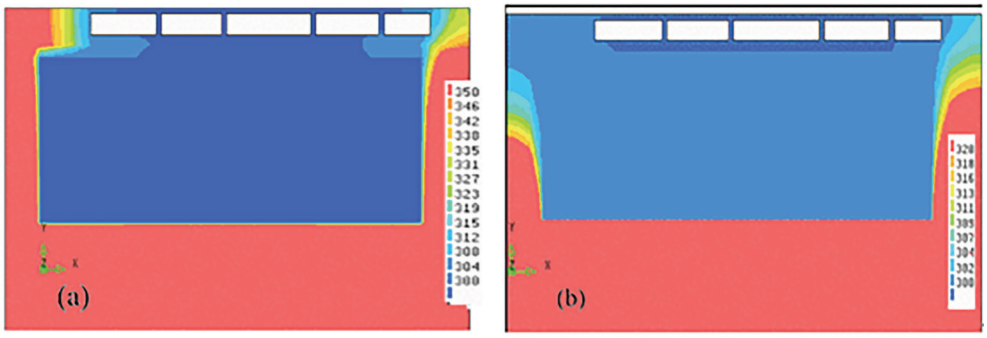

Fig. 18 Temperature distribution with diffusion only (a) and with forced convection (b) (Reprinted with permission from [117])

analysis, it is found that the removal rate of impurities can be improved to a certain extent in the presence of forced convection. Since the calculation model ignores some influencing factors, such as the temperature gradient that occurs in the molten metal and the condenser in the experiment, the accuracy of the model remains to be verified.

With the development of science and technology, computer simulation has quickly become a research hotspot because of its simplicity, convenience and accuracy. The simulation also solves the problem of atomic level reaction process that cannot be observed by the eye in experiments. What is more, feasibility analysis and theoretical support are made for practical experiments. However, due to the need to make assumptions about the experimental environment in the simulation, the errors caused by the environment and human behavior in the experiment are ignored in many aspects. Therefore, there are discrepancies between the simulation results and the experimental results, which is also a direction for future researches.

6 Conclusions and outlook

(1) To meet the demand for high-purity metals in high-precision industries, in recent years, researchers have innovated new ideas and investigated new technologies. Efficient, clean and environmentally friendly experimental routes are developed. This paper mainly summarizes the technology of preparing high-purity metals by vacuum distillation and discusses the refining principle, distillation device and simulation application of this technology in recent years. A large number of studies have proven that calculating the saturated vapor pressure and separation coefficient of impurities can predict the rectification effect. The molecular mean free path is also one of the key factors to judge the type of distillation process. The type and concentration of impurities, the structure and material of the equipment, the distillation temperature, distillation time, vacuum degree and condensation temperature have an impact on the distillation effect. In addition, the evaporation rate of impurities can also indirectly reflect the distillation effect.

(2) Due to the principle of vacuum distillation, it is difficult to have a high removal rate of impurities with similar saturated vapor pressures at the same temperature. It can be separated by taking advantage of the difference in physical or chemical properties between different impurities, which makes up for the shortcomings of vacuum distillation technology to a certain extent.

(3) Some researchers have conducted thermodynamic and dynamics research on vacuum distillation technology. The experimental process is simulated by various model softwares so that the experimenters can better understand the whole process of the experiment. The appropriate experimental parameters should be found to achieve the best vacuum distillation effect. The combination of experiment and simulation calculation will be a hot research direction in the field of vacuum purification.

(4) The optimization of high-purity metal preparation by vacuum distillation can be realized by combining theoretical calculation, experimental process and simulation. It can be used for providing reference in actual production, improving production efficiency, saving production cost and realizing high purification preparation of metal.

CRediT authorship contribution statement

Zhi-peng XU: Conceptualization, Experimental Investigation, Writing − Original draft; **Li-li JIA:** Experimental investigation, Validation, Writing − Original draft; **Zhi-qiang HE:** Experimental investigation, Visualization; **Xue-yi GUO:** Funding acquisition, Writing − Review & editing; **Qing-hua TIAN:** Funding acquisition, Writing − Review & editing.

Declaration of competing interest

The authors declare that they have no known competing financial interests or personal relationships that could have appeared to influence the work reported in this paper.

Acknowledgments

This work was financially supported by the National Natural Science Foundation of China (Nos. 52104355, 52074363, 51922108), and the National Key R&D Program of China (Nos. 2019YFC1907402, 2018YFC1902501).

References

[1] HINRICHS J. High purity aluminium analysis [J]. Aluminium International Today, 2014, 1: 4−5.

[2] MOHAMED S, FRIEDRICH S, FRIEDRICH B. Refining principles and technical methodologies to produce ultra-pure

magnesium for high-tech applications [J]. Metals, 2019, 9: 85.

[3] ZIOUR A, ZAHRAMAN K, ROUMIE M, CHARARA J, FAWAZ A, LMAI F, HAGEALI M. Purification of tellurium to nearly 7N purity [J]. Materials Science and Engineering: B, 2006, 131: 54−61.

[4] GHOSH K, MANI V N, DHAR S. Numerical study and experimental investigation of zone refining in ultra-high purification of gallium and its use in the growth of GaAs epitaxial layers [J]. Journal of Crystal Growth, 2009, 311: 1521−1528.

[5] ZHOU Zhi-hua, RUAN Jian-ming, MO Hong-bing. Preparation of 6N high-purity indium by method of physical-chemical purification and electrorefining [J]. Journal of Materials Science, 2005, 40: 6529−6533.

[6] ESFANDIARPOUR S, BOEHME L, HASTINGS J T. Focused electron beam induced deposition of copper with high resolution and purity from aqueous solutions [J]. Nanotechnology, 2017, 28: 125301.

[7] SOUNDERAJAN S, KUMAR G K, UDAS A C, MUKHERJEE T. In situ matrix volatilization for trace element determination in high purity antimony and antimony oxide and elucidation of the atomization mechanisms by ETAAS [J]. Atomic Spectroscopy, 2013, 34: 181−190.

[8] LIU Yuan, ZHENG Ya-jie, SUN Zhao-ming. Preparation of high purity cadmium with micro-spherical architecture from zinc flue dust [J]. Transactions of Nonferrous Metals Society of China, 2015, 25: 2073−2080.

[9] TAMURA Y, YANAGISAWA T, HAITANI T, TAMEHIRO H, KONO N, SODA H, MCLEAN A. Room temperature deformation properties of high purity AZ31 magnesium alloy [J]. Canadian Metallurgical Quarterly, 2007, 46: 455−466.

[10] TAKAJO S, YAMASHITA T, MATSUZAKI A, KONDO O. Excellent plasticity revealed in high purity Si steels by the addition of Cr [J]. International Journal of Materials Research, 2021, 93: 42−47.

[11] ASAHINA M, HARIMA N, TAKAKI S, ABIKO K. High-temperature mechanical properties of a high-purity Cr−Ni alloy [J]. Materials Transactions, 2000, 41: 178−183.

[12] January to December of 2021 Metals Balances [R]. United Kingdom: Statistics World Bureau of Metal, 2022/10/24.

[13] CHENG Zi-yi, LONG Jian-ping, YANG Wu-yong, ZHOU Kun. Study on preparation of high purity tellurium by vacuum distillation [J]. Guangzhou Chemical Industry, 2021, 49: 54−56, 64. (in Chinese)

[14] GUO Xiang. Chemical refining method of high-purity metal [J]. Nonferrous Metals and Rare Earth Applications, 2003, 2: 6−10. (in Chinese)

[15] WANG Kai-fei, ZHANG Guo-hua. Synthesis of high-purity ultrafine tungsten and tungsten carbide powders [J]. Transactions of Nonferrous Metals Society of China, 2020, 30: 1697−1706.

[16] GUO Xiang. Physical refining of high-purity metals [J]. Nonferrous Metals and Rare Earth Applications, 2003, 2: 1−5. (in Chinese)

[17] CHEN Zhong-wei, GAO Jian-ping. Formation of twinned dendrites during unidirectional solidification of Al−32%Zn alloy [J]. Transactions of Nonferrous Metals Society of China, 2018, 28: 802−811.

[18] XU Shun-lei, LIU Zhong-qi, CHANG Yi-chuan, CHENG Geng. Overview of preparation methods of high purity metal tellurium and its oxides [J]. Ship Power Technology, 2019, 30: 46−50. (in Chinese)

[19] YUAN Rui, LI Shao-long, CHE Yu-si, HE Ji-lin, SONG Jian-xun, YANG Bin. A critical review on extraction and refining of vanadium metal [J]. International Journal of Refractory Metals and Hard Materials, 2021, 101: 105696.

[20] WAN He-li. Study on the migration behavior of impurity elements in the process of aluminum purification by zone smelting [D]. Kunming: Kunming University of Science and Technology, 2021. (in Chinese)

[21] FENG Xue-liang. Model and numerical simulation of solid−liquid phase transition model for silicon single crystal growth by Czochralski method [D]. Xi'an: Xi'an University of Technology, 2018. (in Chinese)

[22] POŽEGA E, IVANOV S, STEVIĆ Z, KARANOVIĆ L, TOMANEC R, GOMIDŽELOVIĆ L, KOSTOV A. Identification and characterization of single crystal Bi_2Te_3−Se alloy [J]. Transactions of Nonferrous Metals Society of China, 2015, 25: 3279−3285.

[23] YU Liang, KANG Xiao-an, CHEN Luo-na, LUO Kun, JIANG Yan-li, CAO Xiu-ling. Research status of high-purity metals prepared by zone refining [J]. Materials, 2021, 14: 2064.

[24] GALAZKA Z. Growth of bulk β-Ga_2O_3 single crystals by the Czochralski method [J]. Journal of Applied Physics, 2022, 131: 31103.

[25] TIAN Qing-hua, GAN Xiang-dong, YU Da-wei, CUI Fu-hui, GUO Xue-yi. One-step and selective extraction of nickel from nickel-based superalloy by molten zinc [J]. Transactions of Nonferrous Metals Society of China, 2021, 31: 1828−1841.

[26] JIANG Wen-long, DENG Yong, YANG Bin, LIU Da-chun, DAI Yong-nian, XU Bao-qiang. Application of vacuum distillation in refining crude indium [J]. Rare Metals, 2013, 32: 627−631.

[27] ALCOCK C B, ITKIN V P, HORRIGAN M K. Vapour pressure equations for the metallic elements: 298−2500 K [J]. Canadian Metallurgical Quarterly, 1984, 23: 309−313.

[28] ZHANG Yong-wei, DENG Ju-hai, JIANG Wen-long, MEI Qing-song, LIU Da-chun. Application of vacuum distillation in refining crude lead [J]. Vacuum, 2018, 148: 140−148.

[29] LUO Hu-an, JIANG Wen-long, ZHA Guo-zheng, LIU Lang, ZHEN Tian-tian, YANG Bin, XU Bao-qiang. Removal of impurity Pb during crude selenium purification by controlling potential oxidation and vacuum distillation [J]. Vacuum, 2022, 195: 110674.

[30] KONG Xiang-feng, YANG Bin, XIONG Heng, KONG Ling-xin, LIU Da-chun, XU Bao-qiang. Thermodynamics of removing impurities from crude lead by vacuum distillation refining [J]. Transactions of Nonferrous Metals Society of China, 2014, 24: 1946−1950.

[31] ZHANG Xiao-wei, MIAO Rui-ying, WU Dao-gao, ZHU Qiong, WANG Zhi-qiang, CHEN De-hong, YAN Shi-hong. Impurity distribution in distillate of terbium metal during vacuum distillation purification [J]. Transactions of Nonferrous Metals Society of China, 2017, 27: 1411−1416.

[32] KONG Xiang-feng, YANG Bin, XIONG Heng, LIU Da-chun, XU Bao-qiang. Removal of impurities from crude lead with high impurities by vacuum distillation and its analysis [J]. Vacuum, 2014, 105: 17−20.

[33] CHURBANOV M F, GERASIMENKO V V, SHIRYAEV V S. Behavior of impurity inclusions during vacuum distillation of tellurium [J]. Inorganic Materials, 2001, 37: 1017−1021.

[34] PRASAD D S, MUNIRATHNAM N R, RAO J V, PRAKASH T L. Purification of tellurium up to 5N by vacuum distillation [J]. Materials Letters, 2005, 59: 2035−2038.

[35] ZHA Guo-zheng, YANG Bin, YANG Chong-fang, GUO Xin-yu, JIANG Wen-long. Selective separation and recovery of valuable metals by vacuum distillation of copper anode slime flotation tailings [J]. JOM, 2019, 71: 2413−2419.

[36] FENG Yue-bin, YANG Bin, DAI Yong-nian. Thermodynamics on formation of C, Al_4C_3 and Al_2O_3 in AlCl disproportionation process in vacuum to produce aluminum [J]. Transactions of Nonferrous Metals Society of China, 2014, 24: 3366−3371.

[37] LI Zhi-chao, DENG Ju-hai, LIU Da-chun, JIANG Wen-long, ZHA Guo-zheng, HUANG Da-xin, DENG Pan, LI Bao-le. Waste-free separation and recovery of copper telluride slag by directional sulfidation−vacuum distillation [J]. Journal of Cleaner Production, 2022, 335: 130356.

[38] LU Dian-kun, CHANG Yong-feng, YANG Hong-ying, XIE Feng. Sequential removal of selenium and tellurium from copper anode slime with high nickel content [J]. Transactions of Nonferrous Metals Society of China, 2015, 25: 1307−1314.

[39] GUO Xin-yu, ZHOU Yi, ZHA Guo-zheng, JIANG Wen-long YANG Bin, MA Wen-hui. A novel method for extracting metal Ag and Cu from high value-added secondary resources by vacuum distillation [J]. Separation and Purification Technology, 2020, 242: 116787.

[40] ZHA Guo-zheng, YANG Chong-fang, WANG Yun-ke, GUO Xin-yu, JIANG Wen-long, YANG Bin. New vacuum distillation technology for separating and recovering valuable metals from a high value-added waste [J]. Separation and Purification Technology, 2019, 209: 863−869.

[41] CURTOLO D C, XIONG N, FRIEDRICH S, FRIEDRICH B. High-and ultra-high-purity aluminum, a review on technical production methodologies [J]. Metals, 2021, 11: 1407.

[42] LÜ Kai-li, YANG Feng, XIE Zhi-yun, LIU Hua-shan, CAI Ge-mei, JIN Zhan-peng. Isothermal section of Al−Ti−Zr ternary system at 1073 K [J]. Transactions of Nonferrous Metals Society of China, 2016, 26: 3052−3058.

[43] WANG Meng, LIU Hua-shan, CAI Ge-mei, JIN Zhan-peng. Measurement of phase equilibria in Ti−Ni−Sn system [J]. Transactions of Nonferrous Metals Society of China, 2018, 28: 819−828.

[44] ZHONG Yue, SUN Yue, LIU Hua-shan, CAI Ge-mei, JIN Zhan-peng. Phase equilibria in Ti−Ni−Pt ternary system [J]. Transactions of Nonferrous Metals Society of China, 2018, 28: 574−584.

[45] YANG Bin, KONG Ling-xin, XU Bao-qiang, LIU Da-chun, DAI Yong-nian. Recycling of metals from waste Sn-based alloys by vacuum separation [J]. Transactions of Nonferrous Metals Society of China, 2015, 25: 1315−1324.

[46] YANG Hong-wei, ZHANG Cheng, YANG Bin, XU Bao-qiang, LIU Da-chun. Vapor-liquid phase diagrams of Pb−Sn and Pb−Ag alloys in vacuum distillation [J]. Vacuum, 2015, 119: 179−184.

[47] XU Jun-jie, PANG Jian, KONG Ling-xin, XU Bao-qiang, YANG Bin, REN Jia-qi. Study on vapor−liquid phase equilibrium of Zn−Ni binary alloy in vacuum distillation [J]. The Chinese Journal of Nonferrous Metals, 2022, 32: 218−226. (in Chinese)

[48] XU Shuai, SONG Bing-yi, JIANG Wen-long, YANG Bin. Modeling and calculation of activities of constituent elements in binary alloys [J]. Chinese Journal of Vacuum Science and Technology, 2015, 35: 919−925. (in Chinese)

[49] CHEN Yu-hu, YANG Bin, XU Bao-qiang, YANG Hong-wei. Experimental investigation and modeling of phase equilibria for Cu−Bi and Cu−Bi−Sb alloys in vacuum distillation [J]. Fluid Phase Equilibria, 2019, 490: 86−91.

[50] ODUSOTE Y A, JABAR J M, BOLARINWA H S, AKINBISEHIN A B. Application of molecular interaction volume model in separation of Ti−Al alloys in vacuum distillation [J]. Vacuum, 2019, 169: 108885.

[51] YU Qiang, WU Ji-jun, MA Wen-hui. Using MIVM model to predict the volatilization characteristics of impurities in vacuum refining of metallurgical grade silicon [J]. Journal of Vacuum Science and Technology, 2016, 36: 1193−1199. (in Chinese)

[52] GAO Zhe, KONG Xiang-feng, YI Jia-fei, YANG Bin, XU Bao-qiang, LIU Da-chun, WU Jian, XIONG Heng. Vacuum gasification-directional condensation for separation of tellurium from lead anode slime [J]. Metals, 2021, 11: 1535.

[53] XIONG Li-zhi, HE Ze-qiang, LIU Wen-ping. Preparation of high-purity bismuth by sulphur deleadization in vacuum distillation [J]. Transactions of the Nonferrous Metals Society of China, 2004, 14: 1210−1214.

[54] WANG Ying, CHEN Shao-chun, GU Heng. Preparation method of high-purity tellurium [J]. Journal of Guangdong Nonferrous Metals, 2002(1): 51−54. (in Chinese)

[55] PRASAD D S, SUDHEER C H, MUNIRATHNAM N R, PRAKASH T L. Tellurium purification: various techniques and limitations [J]. Bulletin of Materials Science, 2002, 25: 545−547.

[56] RODRIGUEZ-ROJAS M J, FRIEDRICH S, FRIEDRICH B. Feasibility of employing the cooled finger, a fractional crystallization method for the purification of magnesium [J]. Journal of Sustainable Metallurgy, 2022, 8: 1276−1289.

[57] FAN Ling-ling, ZHOU Ming-yang, GUO Yang-yang, ZHANG Yu-wen-xi, QUAN Gao-feng. Effect of ECAP process on liquid distribution of AZ80M alloy during semi-solid isothermal heat treatment [J]. Transactions of Nonferrous Metals Society of China, 2021, 31: 1599−1611.

[58] LIU Yuan, ZHANG Hua-wei, LI Yan-xiang. Effect of melt superheat on structural uniformity of lotus-type porous metals prepared by unidirectional solidification [J]. Transactions of Nonferrous Metals Society of China, 2015, 25: 1004−1010.

[59] RONG Mian, ZHANG Liang, WU Guo-hua, LI Wei-wei, ZHANG Xiao-long, SUN Jiang-wei, DING Wen-jiang. Effect of refining processes on inclusions and mechanical properties of cast Al−2Li−2Cu−0.2Zr alloy [J]. Transactions

of Nonferrous Metals Society of China, 2019, 29: 1375−1382.

[60] WANG Yao-wu, PENG Jian-ping, DI Yue-zhong. Separation and recycling of spent carbon cathode blocks in the aluminum industry by the vacuum distillation process [J]. JOM, 2018, 70: 1877−1882.

[61] LIANG Dong, TIAN Yang, YANG Bin, XIONG Neng, WANG Fei, XU Bao-qiang. One-step preparation of high purity magnesium by vacuum distillation technology [J]. Vacuum, 2021, 192: 110464.

[62] YUAN Tie-wen. Variable volume multistage tower vacuum distillation furnace [J]. Yunnan Metallurgy, 1981(4): 34−37. (in Chinese)

[63] HAGEMAN A M, HARRISON M J, FRITZ N, KREHBIEL T N, WHITE R, PATENAUDE J, MCGREGOR D S. Purification of tellurium to 6N using a multistage vacuum distillation method [C]// Applications VIII SPIE. San Diego, USA, 2007: 259−265.

[64] ZHA Guo-zheng, WANG Yun-ke, CHENG Min-qiang, HUANG Da-xin, JIANG Wen-long, XU Bao-qiang, YANG Bin. Purification of crude selenium by vacuum distillation and analysis [J]. Journal of Materials Research and Technology, 2020, 9: 2926−2933.

[65] DENG Ju-hai, ZHANG Yong-wei, JIANG Wen-long, MEI Qing-song, LIU Da-chun. Harmless, industrial vacuum-distillation treatment of noble lead [J]. Vacuum, 2018, 149: 306−312.

[66] CHEN Ming-baio, WANG Xiao-min, LIU Ri-ping, YANG Qing-xiang, LIU Wen-chang, TAO You-sheng, YAN Jun, MA Xiao-yi, LI Jian, ZHAI Pan-pan. Methods and equipment of vacuum and electromagnetism suspending distillation for fine of non-ferrous metals [J]. Advanced Materials Research, 2011, 295/296/297: 1150−1155.

[67] ZHANG Xiao-feng, LIU Da-chun, JIANG Wen-long, XU Wen-jie, DENG Pan, DENG Ju-hai, YANG Bin. Application of multi-stage vacuum distillation for secondary resource recovery: Potential recovery method of cadmium telluride photovoltaic waste [J]. Journal of Materials Research and Technology, 2020, 9: 6977−6986.

[68] LI Dong-sheng, DAI Yong-nian, YANG Bin, LIU Da-chun, DENG Yong. Purification of indium by vacuum distillation and its analysis [J]. Journal of Central South University, 2013, 20: 337−341.

[69] XIONG Neng, FRIEDERICH S, MOHAMED S R, KIRILLOV L, YE Xiao-zhou, TIAN Yang, FRIEDRICH B. The separation behavior of impurities in the purification of high-purity magnesium via vacuum distillation [J]. Journal of Sustainable Metallurgy, 2022, 8(4): 1561−1572.

[70] GUO Xue-yi, ZHANG Lei, TIAN Qing-hua, YU Da-wei, SHI Jing, YI Yu. Selective removal of As from arsenic-bearing dust rich in Pb and Sb [J]. Transactions of Nonferrous Metals Society of China, 2019, 29: 2213−2221.

[71] KHALIQ A, ALI H T, YUSUF M. Thermodynamic and kinetic analysis of CrB_2 and VB_2 formation in molten Al−Cr−V−B alloy [J]. Transactions of Nonferrous Metals Society of China, 2021, 31: 3162−3176.

[72] ZOU Tian-peng, YU Gao-yang, CHEN Shu-hai, HUANG Ji-hua, YANG Jian, ZHAO Zhi-yi, RONG Ji-ping, YANG Jin. Effect of Si content on interfacial reaction and properties between solid steel and liquid aluminum [J]. Transactions of Nonferrous Metals Society of China, 2021, 31: 2570−2584.

[73] NIU Zhi-wei, HUANG Ji-hua, CHEN Shu-hai, ZHAO Xing-ke. Effects of germanium additions on microstructures and properties of Al−Si filler metals for brazing aluminum [J]. Transactions of Nonferrous Metals Society of China, 2016, 26: 775−782.

[74] VIDYASAGAR C H S, KARUNAKAR D B. Effects of yttrium addition and aging on mechanical properties of AA2024 fabricated through multi-step stir casting [J]. Transactions of Nonferrous Metals Society of China, 2020, 30: 288−302.

[75] XIA Yu, WU Liang, YAO Wen-hui, HAO Meng, CHEN Jing, ZHANG Cheng, WU Tao, XIE Zhi-hui, SONG Jiang-feng, JIANG Bin, MA Yan-long, PAN Fu-sheng. In-situ layered double hydroxides on Mg−Ca alloy: Role of calcium in magnesium alloy [J]. Transactions of Nonferrous Metals Society of China, 2021, 31: 1612−1627.

[76] STEINACHER M, MRVAR P, ZUPANIČ F. Interaction between AE44 magnesium alloy and $SiC−Al_2O_3−SiO_2$ ceramic foam [J]. Transactions of Nonferrous Metals Society of China, 2015, 25: 1011−1019.

[77] HUANG Hai-feng, LIU Zhi-jian, LIANG Chao-ping, CHEN Li-bao. Age softening phenomenon and microscopic mechanism of Li−B alloy [J]. Transactions of Nonferrous Metals Society of China, 2020, 30: 2491−2501.

[78] SUN Zhao-ming, ZHENG Ya-jie. Preparation of high pure tellurium from raw tellurium containing Cu and Se by chemical method [J]. Transactions of Nonferrous Metals Society of China, 2011, 21: 665−672.

[79] JIANG Zhong-tao, JIANG Bin, ZHANG Jian-yue, DAI Jia-hong, YANG Qing-shan, YANG Qin, PAN Fu-sheng. Effect of Al_2Ca intermetallic compound addition on grain refinement of AZ31 magnesium alloy [J]. Transactions of Nonferrous Metals Society of China, 2016, 26: 1284−1293.

[80] WANG Bo, XUE Song-bai, MA Chao-li, HAN Yi-long, LIN Zhong-qiang. Effect of combinative addition of Ti and Sr on modification of AA4043 welding wire and mechanical properties of AA6082 welded by TIG welding [J]. Transactions of Nonferrous Metals Society of China, 2017, 27: 272−281.

[81] JEVTIC D, VITOROVIC D. A new procedure for the preparation of antimony of high purity combined with the production of antimony trioxide of high purity [J]. Industrial and Engineering Chemistry Product Research and Development, 1974, 13: 275−279.

[82] ZHANG X X, FRIEDRICH S, FRIEDRICH B. Separation behavior of arsenic and lead from antimony during vacuum distillation and zone refining [J]. Journal of Materials Research and Technology, 2020, 9: 4386−4398.

[83] ZHAO Peng-cheng, SHEN Yi-fu, HUANG Guo-qiang, ZHENG Qi-xian. Numerical simulation of friction stir butt-welding of 6061 aluminum alloy [J]. Transactions of Nonferrous Metals Society of China, 2018, 28: 1216−1225.

[84] YAO Xin-xin, LI Jian-yu, WANG Yi-fei, GAO Xiang, ZHANG Zhao. Numerical simulation of powder effect on solidification in directed energy deposition additive manufacturing [J]. Transactions of Nonferrous Metals

Society of China, 2021, 31: 2871−2884.

[85] CHEN Zhi, CHEN Pei, GONG He-he, DUAN Pei-pei, HAO Li-mei, JIN Ke-xin. Phase field method simulation of faceted dendrite growth with arbitrary symmetries [J]. Transactions of Nonferrous Metals Society of China, 2018, 28: 290−297.

[86] DEWANG Y, HORA M S, PANTHI S K. Prediction of crack location and propagation in stretch flanging process of aluminum alloy AA-5052 sheet using FEM simulation [J]. Transactions of Nonferrous Metals Society of China, 2015, 25: 2308−2320.

[87] KRAVCHENKO A. Equation of impurity distribution in solidified distillates [J]. Inorganic Materials, 2007, 43: 916−917.

[88] PAPIROV I I, KRAVCHENKO A I, MAZIN A I, SHIYAN A V, VIRICH V D. Impurity distribution in a magnesium sublimate [J]. Inorganic Materials, 2015, 51: 563−565.

[89] ZHANG Xiao-wei, MIAO Rui-ying, LI Chuan-jun, WU Dao-gao, YAN Huan, WANG Zhi-qiang, CHEN De-hong, YAN Shi-hong, LI Zong-an. Impurity distribution in metallic dysprosium during distillation purification [J]. Journal of Rare Earths, 2016, 34: 924−930.

[90] ZHANG Lei, ZHANG Xiao-wei, LI Zong-an, CHEN De-hong, WANG Zhi-qiang, PANG Si-ming, ZHOU Lin, WU Dao-gao, KE Ling-sheng, NAN Chang-bin. Distribution model of lowly volatile impurity in rare earth metal purified by vacuum distillation [J]. Separation and Purification Technology, 2021, 262: 118314.

[91] ZHANG Lei, ZHANG Xiao-wei, LI Zong-an, PANG Si-ming, WANG Zhi-qiang, CHEN De-hong, WU Dao-gao, YANG Bing-zheng. Distribution model of highly volatile impurity in distillate of rare earth metal [J]. Vacuum, 2020, 176: 109307.

[92] LEE D H, JEOUNG H J, LEE T H, YI K W, LEE J Y, KIM Y M, OKABE T H, KANG J. Scale-up study of molten salt electrolysis using Cu or Ag cathode and vacuum distillation for the production of high-purity Mg metal from MgO [J]. Journal of Sustainable Metallurgy, 2021, 7: 883−897.

[93] LUO Huan, ZHA Guo-zheng, LIU Lang, JIANG Wen-long, ZHEN Tian-tian, XIONG Heng, YANG Bin, DENG Tong-da, XU Bao-qiang. Sustainable and clean approach to remove high toxicity element from high-value waste selenium material [J]. Journal of Sustainable Metallurgy, 2022, 8: 112−121.

[94] ZHEN Tian-tian, LUO Huan, LIU Lang, ZHA Guo-zheng, YANG Bin, JIANG Wen-long, XU Bao-qiang. Selective recovery of valuable metals (Se, Te, Cu) from the selenium distillation residue by sulfuric acid oxidative leaching [J]. Journal of Sustainable Metallurgy, 2022, 8: 1191−1203.

[95] LI Hong, WU Yan, LI Xin-gang. State-of-the-art of advanced distillation technologies in China [J]. Chemical Engineering & Technology, 2016, 39: 815−833.

[96] TIAN Ze-an, ZHOU Li-li, MO Yun-fei, LIANG Yong-chao, LIU Rang-su. Cooling rate dependence of polymorph selection during rapid solidification of liquid metal zinc [J]. Transactions of Nonferrous Metals Society of China, 2015, 25: 4072−4079.

[97] SUN Bao-jun, XIAO Bing. Mechanical properties of diamond grinding discs brazed in a continuous-belt tunnel furnace or vacuum furnace [J]. The International Journal of Advanced Manufacturing Technology, 2017, 89: 1379−1386.

[98] BAO Lei, ZHANG Zhi-qiang, LE Qi-chi, RU Li-li, CUI Jian-zhong. Heat transfer behavior of AZ80-1%Y alloy during low-frequency electromagnetic casting [J]. Transactions of Nonferrous Metals Society of China, 2015, 25: 3618−3624.

[99] BABAEE M H, NIROUMAND B, MALEKI A, ZAND M L. Simulation and experimental verification of interfacial interactions in compound squeeze cast Al/Al−Cu macrocomposite bimetal [J]. Transactions of Nonferrous Metals Society of China, 2019, 29: 950−963.

[100] CHEN Lin, CHEN Peng, ZHANG Du-chao, LIU Wei-feng, YANG Tian-zu. Thermodynamic simulation of complex Pb−Bi concentrate oxidative bath smelting process [J]. Transactions of Nonferrous Metals Society of China, 2021, 31: 1165−1174.

[101] MIAO Ze-lin, ZHAN Jing, XU Zi-wei. Thermodynamic simulation of metal behaviors in Cu^{2+}–Ni^{2+}–NH_3–NH^{4+}–$C_2O_4^{2-}$–H_2O system [J]. Transactions of Nonferrous Metals Society of China, 2021, 31: 1475−1483.

[102] DONG Guo-jiang, ZHAO Chang-cai, YA Yuan-yuan, ZHAO Jian-pei. Discrete element and finite element coupling simulation and experiment of hot granule medium pressure forming [J]. Transactions of Nonferrous Metals Society of China, 2015, 25: 4089−4101.

[103] ZHANG Fu-yuan, ZHENG Ya-jie, PENG Guo-min. Selection of reductants for extracting selenium and tellurium from degoldized solution of copper anode slimes [J]. Transactions of Nonferrous Metals Society of China, 2017, 27: 917−924.

[104] ZHANG Bei-kai, GUO Xue-yi, WANG Qin-meng, TIAN Qing-hua. Thermodynamic analysis and process optimization of zinc and lead recovery from copper smelting slag with chlorination roasting [J]. Transactions of Nonferrous Metals Society of China, 2021, 31: 3905−3917.

[105] LI H, KIM W G, YOO B W, PARK K T, LEE H H, CHOI J C, HONG S J, KONG M S, LEE H Y, LEE J H. Numerical analysis and experimental validation of distillation process for purification of tellurium [J]. Separation Science and Technology, 2014, 49: 197−208.

[106] ZHANG Xiao-wei, MIAO Rui-ying, CHEN De-hong, WANG Zhi-qiang, LI Zong-an, YAN Shi-hong, JIN Xiao-li. Numerical simulation during vacuum sublimation purification of metal Tm (I): Model foundation and validation [J]. Journal of Rare Earths, 2013, 31: 180−185.

[107] LIU Ri-xin, DAI Yong-nian. Pure metal vacuum distillation Research (I): Mathematical model [J]. Vacuum Science and Technology, 1996, 16: 134−139. (in Chinese)

[108] XU Wei-de, ZANG Jun-feng, ZHANG Ri-dong. Application of multi-model switching predictive functional control on the temperature system of an electric heating furnace [J]. ISA Trans, 2017, 68: 287−292.

[109] WANG Yue-fei, LIU Zhen. Development of numerical modeling and temperature controller optimization for internal heating vacuum furnace [J]. IEEE Access, 2021, 9: 126765−126773.

[110] HAGER J P, WALKER R A. Galvanic cell studies using a molten oxide electrolyte: Part I—Thermodynamic properties of the lead-silver system [J]. Trans Met Soc AIME, 1968,

242: 183.
[111] KAZANC S. Molecular dynamics study of pressure effect on crystallization behavior of amorphous CuNi alloy during isothermal annealing [J]. Physics Letters A, 2007, 365: 473−477.
[112] ZHAO Wei-chen, XU Bao-qiang, YANG Bin, YANG Hong-wei. Study on evaporation kinetics of Zn in Bi−Zn and Bi−Sn−Zn systems under vacuum condition [J]. Journal of Sustainable Metallurgy, 2021, 7: 995−1003.
[113] YANG Hong-ying, LI Xue-jiao, TONG Lin-lin, JIN Zhe-nan, YIN Lu, CHEN Guo-bao. Leaching kinetics of selenium from copper anode slimes by nitric acid−sulfuric acid mixture [J]. Transactions of Nonferrous Metals Society of China, 2018, 28: 186−192.
[114] LIU Wei, WU Bo-qiang, LIU Hai-rong, LIU Rang-su, MO Yun-fei, TIAN Ze-an, HOU Zhao-yang, XI Ting-fei, WAN Zhi-yi, HUANG Chang-xiong, CHEN Xin. Simulation on microstructure evolution and mechanical properties of Mg−Y alloys: Effect of trace Y [J]. Transactions of Nonferrous Metals Society of China, 2022, 32: 812−823.
[115] JIA Guo-bin, LIU Yuan-yuan, YANG Bin, LIU Da-chun. Molecular dynamics simulation on thermodynamic properties of Pb−Ag alloys [J]. Rare Metals, 2010, 29: 323−326.
[116] LI Lin-feng, ZHANG XUE-feng. Molecular dynamics simulation of thermodynamic properties for Al−Si alloys in material manufacturing engineering [J]. Advanced Materials Research, 2012, 583: 326−329.
[117] JALILI V, BAILEY C, PATEL M K. A computational fluid dynamics (CFD) analysis of the vacuum de-zincing process [C]// Proceedings of ASME 2003 on Heat Transfer Summer Conference. Las Vegas, Nevada, UAS, 2003: 361−365.

真空蒸馏制备高纯金属的研究进展

许志鹏，贾莉犁，何志强，郭学益，田庆华

中南大学 冶金与环境学院，长沙 410083

摘　要：随着科学技术的发展，高新技术产业对金属的纯度要求越来越高。然而，痕量杂质的存在会对金属的性能产生不良影响。真空蒸馏工艺因其金属回收率高、环保性能好、设备简单等优点，被广泛应用于制备高纯金属。本文作者围绕真空蒸馏的原理和工艺，系统地总结了高纯金属制备的总体进展。介绍了真空蒸馏的原理、真空蒸馏炉的改进设计、参数优化和仿真模拟。根据该技术制备高纯金属的现状，指出在科学研究中机理研究和仿真模拟是必不可少的。本研究对提高生产效率、节约生产成本及提高金属纯度具有一定的借鉴意义。

关键词：真空蒸馏；高纯金属；理论计算；工艺研究；模拟

(Edited by Wei-ping CHEN)